

Realizing \mathcal{PT} -symmetric BEC subsystems in closed hermitian systems

Robin Gutöhrlein, Jan Schnabel, Ibrokhim Iskandarov, Holger Cartarius, Jörg Main and Günter Wunner

1. Institut für Theoretische Physik, Universität Stuttgart, 70550 Stuttgart, Germany

E-mail: Robin.Gutoehrlein@itp1.uni-stuttgart.de

Abstract. In open double-well Bose-Einstein condensate systems which balance in- and outfluxes of atoms and which are effectively described by a non-hermitian \mathcal{PT} -symmetric Hamiltonian \mathcal{PT} -symmetric states have been shown to exist. \mathcal{PT} -symmetric states obey parity and time reversal symmetry. We tackle the question of how the in- and outfluxes can be realized and introduce a hermitian system in which two \mathcal{PT} -symmetric subsystems are embedded. This system no longer requires an in- and outcoupling to and from the environment. We show that the subsystems still have \mathcal{PT} -symmetric states. In addition we examine what degree of detail is necessary to correctly model the \mathcal{PT} -symmetric properties and the bifurcation structure of such a system. We examine a four-mode matrix model and a system described by the full Gross-Pitaevskii equation in one dimension. We see that a simple matrix model correctly describes the qualitative properties of the system. For sufficiently isolated wells there is also quantitative agreement with the more advanced system descriptions. We also investigate which properties the wave functions of a system must fulfil to allow for \mathcal{PT} -symmetric states. In particular the requirements for the phase difference between different parts of the system are examined.

PACS numbers: 03.75.Kk, 11.30.Er, 03.65.Ge

1. Introduction

In conventional quantum mechanics hermitian operators are used to describe closed quantum systems. These operators allow only for real eigenvalues, which can represent physical observables. Since systems in the real world are hardly ever completely isolated, the environment must be taken into account. Due to a lack of knowledge about the actual layout of the environment of a system or because the environment is too complicated to be completely calculated, one can effectively describe such systems as open quantum systems as long as the interaction to the environment is known. Such Hamiltonians are often no longer hermitian. The interaction with the environment, e.g. gain and loss of the probability amplitude, that is the wave function, can be expressed by complex potentials [1]. These Hamiltonians in general do not have a real eigenvalue spectrum.

A special class of non-hermitian operators was investigated by Bender and Boettcher in 1998 [2]. For certain parameter ranges these operators also had purely real eigenvalue spectra. The origin of the special property can be traced back to the \mathcal{PT} -symmetry of the operator, where the \mathcal{PT} -operator consists of the parity operator \mathcal{P} and the time reversal operator \mathcal{T} . The parity operator exchanges $\hat{x} \rightarrow -\hat{x}$ and $\hat{p} \rightarrow -\hat{p}$. The time reversal operator replaces $\hat{p} \rightarrow -\hat{p}$ and $i \rightarrow -i$. A \mathcal{PT} -symmetric system has a Hamiltonian which fulfils $[H, \mathcal{PT}] = 0$. For a system with

$$H = -\Delta + V \quad (1)$$

the position space representation of the potential must obey the condition

$$V(x) = V^*(-x), \quad (2)$$

i.e. the real part of the potential must be an even function in the spatial coordinate and the imaginary part must be an odd function. \mathcal{PT} -symmetric systems have been studied theoretically for quantum systems [3–6]. However, the concept of \mathcal{PT} -symmetry is not restricted to quantum mechanics. Indeed, the experimental breakthrough was achieved in optical wave guides by Rüter *et al* [7] when in such a system the effects of \mathcal{PT} -symmetry and \mathcal{PT} -symmetry breaking were observed. This has led to a still increasing interest in the topic [8–11], and \mathcal{PT} -symmetric systems have also been studied in microwave cavities [12], electronic devices [13, 14], and in optical [15–24] systems. Also in quantum mechanics the stationary Schrödinger equation was solved for scattering solutions [4] and bound states [5]. Note that it was shown in [25] that the characteristic \mathcal{PT} -symmetric properties are still found when a many-particle description is used.

In [26] it was suggested that \mathcal{PT} -symmetry could also be realized in quantum systems, namely in Bose-Einstein condensates (BECs). The BEC would be captured in a symmetric double-well potential where particles are gained in one well and lost in the other. This loss and gain can then be described by a complex potential coupling the system to the environment.

The time-independent solutions (see Appendix A) of such a \mathcal{PT} -symmetric double-well system can in the simplest possible case [27] be described by the matrix

$$\begin{pmatrix} -g|\psi_1|^2 - i\gamma & v \\ v & -g|\psi_2|^2 + i\gamma \end{pmatrix} \begin{pmatrix} \psi_1 \\ \psi_2 \end{pmatrix} = \mu \begin{pmatrix} \psi_1 \\ \psi_2 \end{pmatrix}, \quad (3)$$

where ψ_1 and ψ_2 represent the occupations of the two wells with atoms in the condensed phase and μ is the chemical potential. This description can be derived from a non-hermitian representation of a many-particle Bose-Hubbard dimer [28]. The off-diagonal elements v of the matrix describe the couplings between the wave functions in the two potential wells. The diagonal contains a nonlinear entry introducing the particle-particle interaction described by an s-wave scattering process. Its strength can be changed via the parameter g which is proportional to the s-wave scattering length and its physical variation can be achieved close to Feshbach resonances. In comparison to the original model from [27] the replacement $g \rightarrow -g$ is introduced to be consistent with the other models which will be shown later on. In addition the diagonal contains an

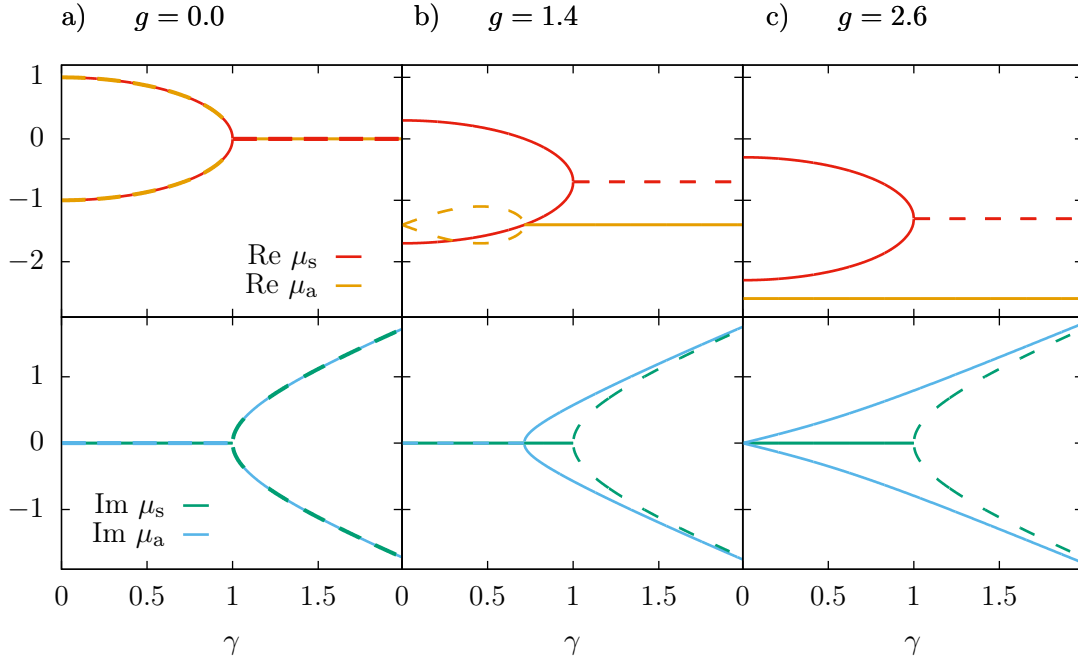


Figure 1. Analytic solutions for the chemical potential (4) of the two-dimensional matrix model described in (3). The coupling strength $v = 1$, and the nonlinearities $g = 0$ in a), $g = 1.4$ in b) and $g = 2.6$ in c) are used. The analytically continued solutions are plotted using dashed lines.

imaginary term with the parameter γ . This term models a particle gain in one well and a particle loss in the other. This gain and loss is provided by the (not further described) environment. The wave functions consist of two complex values and contain no spatial information. Therefore the parity operator \mathcal{P} , which normally exchanges \hat{x} with $-\hat{x}$, exchanges ψ_1 with ψ_2 and vice versa. It is also assumed that the potential wells are isolated enough such that the nonlinear interaction between ψ_1 and ψ_2 can be neglected.

The system (3) is solved analytically [27] for wave function vectors ψ which are normalized to one. The chemical potential reads

$$\begin{aligned}\mu_s &= -\frac{g}{2} \pm \sqrt{v^2 - \gamma^2}, \\ \mu_a &= -g \pm \gamma \sqrt{\frac{4v^2}{g^2 + 4\gamma^2} - 1}.\end{aligned}\tag{4}$$

The values μ_s in (4) are the \mathcal{PT} -symmetric solutions, and the \mathcal{PT} -broken solutions of the system are denoted μ_a . All solutions are shown in figure 1. For small γ the system without nonlinearity ($g = 0$) shows only \mathcal{PT} -symmetric states with real chemical potential $\mu \in \mathbb{R}$ as can be observed in figure 1a. These states pass through a tangent bifurcation at $\gamma = \gamma_c = 1$, and two \mathcal{PT} -broken states emerge. For $\gamma > \gamma_c$ only \mathcal{PT} -broken states with a complex chemical potential $\mu \in \mathbb{C}$ exist.

For a nonlinearity $g > 0$ the bifurcation in which the two \mathcal{PT} -broken states are created moves to a smaller value of γ on one of the \mathcal{PT} -symmetric branches (compare

figure 1b). A pitchfork bifurcation is formed. Thus for nonzero values of g there is an additional parameter region for γ , in which \mathcal{PT} -symmetric and \mathcal{PT} -broken states exist simultaneously. When the nonlinearity is increased even further ($g > 2$) we see in figure 1c that the pitchfork bifurcation is no longer present and the \mathcal{PT} -broken states exist for all values of γ . A thorough examination of the bifurcation structure and of the associated exceptional points can be found in [29].

The matrix model does not take the spatial extension of the system into account. In general BECs can be described by the nonlinear Gross-Pitaevskii equation [30]. Often δ functions have been used to gain a deeper insight [4, 5, 31–41]. Therefore a simple model to include spatial effects describes the potential with double- δ functions [42]. In this system two δ -wells exist at the positions $x = \pm b$. While both of these wells have the same real depth they possess antisymmetric imaginary parts. That is, one well has a particle gain and the other has an equally strong particle drain. The potential fulfils the \mathcal{PT} -symmetry condition (2) and the corresponding Gross-Pitaevskii equation is

$$-\psi''(x) - [(1 + i\gamma)\delta(x + b) + (1 - i\gamma)\delta(x - b)]\psi(x) - g|\psi(x)|^2\psi(x) = \mu\psi(x). \quad (5)$$

In this system \mathcal{PT} -symmetric solutions and \mathcal{PT} -symmetry breaking were found.

In [43, 44] a similar two well system was examined in much greater detail by using a more realistic potential well shape. The Gross-Pitaevskii equation of such a BEC can be written as

$$(-\Delta + V(x) - g|\psi(x, t)|^2)\psi = \mu\psi \quad (6)$$

with the complex potential

$$V(x) = \frac{1}{4}x^2 + V_0^G e^{-\sigma x^2} + i\gamma x e^{-\rho x^2} \quad \text{with } \rho = \frac{\sigma}{2 \ln(4V_0^G \sigma)} \quad (7)$$

containing the BEC in a harmonic trap divided by a Gaussian potential barrier into two wells. The parameter ρ is chosen in such a way that the maximal coupling between the subsystems occurs at the minima of the potential wells. The stationary states show the same general behaviour as those in the matrix model.

All descriptions so far used complex potentials to effectively describe the environment. Therefore only the \mathcal{PT} -symmetric part of the whole system was described in detail while the concrete layout of the environment itself was not specified. We will now discuss how it might be possible to embed such a \mathcal{PT} -symmetric two-well system into a larger hermitian system and therefore explicitly include the environment into our description.

As a first step in this direction a hermitian four well model was used [45, 46], where the double-well with in- and outgoing particle fluxes is achieved by embedding it into the larger system. The two outer wells have time-dependent adjustable parameters namely the potential depth and the coupling strength to the inner wells. By lowering and raising these wells a particle gain and loss in the two inner wells can be obtained, which exactly corresponds to the loss and gain in the non-hermitian two-well model. However, the \mathcal{PT} -symmetric subsystem of the inner wells loses its properties when the

well which provides the particle gain is depleted. A second possible realization was suggested in [47], where the wave function of a double-well potential was coupled to additional unbound wave functions (e.g. one ingoing and one outgoing) connecting the gain and loss of the system with a reservoir. These auxiliary wave functions replace the previously unknown environment of the system.

In this paper we propose an additional way of realizing a \mathcal{PT} -symmetric two-well system by extending the approach used in [47]. We couple two *stationary* bound wave functions, where each of them has the shape of that of the corresponding \mathcal{PT} -symmetric system and their combination results in a hermitian system. The influx from one system originates from the second and vice versa. By tuning the coupling strength between the two systems we will be able to control the gain and loss in the subsystems. In contrast to [47] our systems are closed and do not require incoming or outgoing wave functions or time-dependent potentials. We will show that for suitable states the subsystems are indeed \mathcal{PT} -symmetric, however, also \mathcal{PT} -symmetry breaking can be observed.

In section 2 a four-dimensional matrix model will be constructed similar to the model (3) to observe the general structure of the eigenstates and to determine their \mathcal{PT} -symmetric properties. For this model analytical solutions can be found. In a next step a Hamiltonian is constructed to combine two subsystems with a spatial resolution in one dimension for the wave function similar to the double- δ -potential used in (5). In these systems effects which depend on the shape of the wave functions can be observed. We will examine which detail of description is necessary to capture the \mathcal{PT} -symmetric properties of the system and the bifurcation structure. Since a model with double- δ -potentials is only a rough approximation of the reality we will also introduce an additional system. This system is constructed by coupling two subsystems of the form (6). It not only has an expanded wave function, which resolves spatial information, but also possesses more realistic extended potential wells. In addition the coupling between the two modes takes place over an extended area of space and is not confined to the locations of the δ -wells.

Subsequently we will compare the results obtained with the different descriptions in section 3. We will also compare the bifurcation structure with the model (3). In addition the influence of the phase difference between the two subsystems on the stationary states will be determined. A summary and discussion of the results is given in section 4.

2. Coupling of two two-well potentials in one hermitian system

In figure 2 the layout of two coupled two-well systems is sketched. The two subsystems are labelled A and B and each contains two wells with the labels 1 and 2. In the drawing the potentials of the wells are extended. This corresponds to an ansatz as shown in (6) and (7) and will be one of the systems studied in this work. Each of the wells is coupled to its counterpart in the other subsystem. The coupling strength is described by the parameter γ . Since the strength of the in- and outcoupling is also determined by the wave function of the other subsystem, \mathcal{PT} -symmetry can only exist for both subsystems.

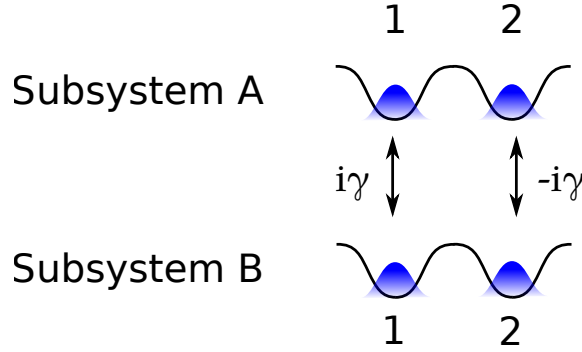


Figure 2. This sketch illustrates how two double-well subsystems are combined into a closed hermitian system. The coupling and description of the wells is given with a varying degree of detail for the different systems discussed in this paper.

There is no \mathcal{PT} -symmetry for arbitrary states but only for states with an appropriate symmetry. As mentioned in the introduction we will investigate the setup in three different degrees of detail.

There exist various other systems which have four distinguished modes. A family of such systems named plaquettes was examined [48, 49]. These systems are seen as a first step towards building \mathcal{PT} -symmetric lattice systems [50, 51]. The plaquettes exist in various configurations which differ in the coupling between the sites. In contrast to the model proposed in this paper the gain and loss in these plaquettes is still provided by non-hermitian terms.

2.1. Four-dimensional matrix model

In a first step we construct the four-dimensional hermitian matrix model. Therefore we place two matrices of the shape (3) on the main diagonal blocks in our new matrix M and remove the terms which couple the system to the environment. They are replaced with coupling terms in the off-diagonal 2×2 matrix-blocks, i.e.

$$M = \left(\begin{array}{cc|cc} -g|\psi_{A,1}|^2 & v & -i\gamma & 0 \\ v & -g|\psi_{A,2}|^2 & 0 & +i\gamma \\ \hline +i\gamma & 0 & -g|\psi_{B,1}|^2 & v \\ 0 & -i\gamma & v & -g|\psi_{B,2}|^2 \end{array} \right) \quad (8)$$

with the wave function

$$\psi = (\psi_{A,1}, \psi_{A,2}, \psi_{B,1}, \psi_{B,2}). \quad (9)$$

The elements of ψ are four complex values with no information about the spatial extension of the wave function. The first two values $\psi_{A,1}, \psi_{A,2} \in \mathbb{C}$ represent the wave function amplitudes in the double-well potential of subsystem A while the values $\psi_{B,1}, \psi_{B,2} \in \mathbb{C}$ represent the amplitudes in the subsystem B. Therefore in this context

the parity operator \mathcal{P} exchanges $\psi_{A,1}$ with $\psi_{A,2}$ and $\psi_{B,1}$ with $\psi_{B,2}$. The two diagonal submatrices will form our subsystems A and B each with two wells indicated by the indices 1 and 2. The first well of subsystem A is coupled via $M_{1,3} = -i\gamma$ to the first well in subsystem B. The first well of subsystem B is coupled via $M_{3,1} = i\gamma$ to $\psi_{A,1}$, therefore keeping the matrix hermitian. The second wells are coupled in a similar manner but with opposite signs. Note that the coupling terms do not yet guarantee a symmetric gain and loss in a subsystem since the gain and loss depend also on the value of the wave function of the other mode.

The coupling between the potential wells in one subsystem is done via the parameter v . The parameter g still describes the particle-particle scattering in one well, but no scattering between the overlap of the wave functions from different wells is taken into account.

The time-independent equation describing the stationary states of the complete system reads

$$M\psi = \mu\psi \quad (10)$$

with real eigenvalues $\mu \in \mathbb{R}$ because the matrix M is hermitian. Since we are also interested in the \mathcal{PT} -symmetric properties of the subsystems we extend (10) to

$$M\psi = \begin{pmatrix} M_A & M_C \\ M_C^* & M_B \end{pmatrix} \begin{pmatrix} \psi_A \\ \psi_B \end{pmatrix} = \begin{pmatrix} \mu_A \psi_A \\ \mu_B \psi_B \end{pmatrix} \quad (11)$$

with independent eigenvalues $\mu_i \in \mathbb{C}$ for both subsystems and

$$M_C = \begin{pmatrix} -i\gamma & 0 \\ 0 & i\gamma \end{pmatrix}, \quad M_i = \begin{pmatrix} -g|\psi_{i,1}|^2 & v \\ v & -g|\psi_{i,2}|^2 \end{pmatrix} \quad (12)$$

for $i = A, B$. We can interpret (11) as two separate equations for both subsystems where the gain and loss is provided by the other subsystem via the matrix M_C . For $\mu_{A,B} \in \mathbb{C}$ this also allows for \mathcal{PT} -broken states where the norm of the subsystems is no longer maintained, but is increased or decreased. Such solutions are therefore non-stationary states, but because the particle number of the whole system is conserved, there is no unlimited exponential growth or decay possible. Therefore these solutions describe only the onset of their growing or decaying temporal evolution. Only states with $\mu_A = \mu_B \in \mathbb{R}$ are stationary \mathcal{PT} -symmetric solutions. For $\mu_A = \mu_B^*$ (11) leads to solutions where the gain and loss of subsystem A (represented by $\text{Im } \mu_A$) is compensated by the loss and gain of subsystem B ($\text{Im } \mu_B$). Therefore the total particle number is indeed conserved.

We can parametrize the ansatz of the wave function for this model and reduce the parameter count by removing a global phase. Solutions exist for different ratios of the probability amplitude between the two subsystems, but they may not exist over the whole range of the parameters. To simplify the equations we choose to restrict the norm

of each subsystem to one. This leads to the ansatz

$$\psi = \begin{pmatrix} \psi_{A,1} \\ \psi_{A,2} \\ \psi_{B,1} \\ \psi_{B,2} \end{pmatrix} = \begin{pmatrix} \cos \theta_A e^{+i\varphi_A} \\ \sin \theta_A e^{-i\varphi_A} \\ \cos \theta_B e^{+i\varphi_B + i\varphi_{\text{rel}}} \\ \sin \theta_B e^{-i\varphi_B + i\varphi_{\text{rel}}} \end{pmatrix} \quad (13)$$

with the parameters θ_A and θ_B determining the distribution of the probability amplitude of the wave function on the two potential wells in one subsystem and the parameters φ_A and φ_B describing the phase difference. The parameter φ_{rel} defines the phase difference between the two subsystems. By applying additional symmetry restrictions and thereby reducing the parameter count even further, analytical solutions of (11) can be obtained and are presented in section 3. All other solutions can be gained numerically by applying a multidimensional root search.

2.2. Model with a spatial resolution of the wave function

We want to know if the basic description provided by the matrix model is sufficient to capture the \mathcal{PT} -symmetric properties and the bifurcation structure of the system or if a more detailed description is necessary. We do this in two steps. First we allow for the more detailed information of a spatially resolved wave function but retain the concept of isolated coupling points. The double- δ system keeps the mathematical and numeric intricacy at bay but still provides a spatial resolution for the wave function. Therefore we combine two systems with δ -potentials (5) which describe each subsystem in one spatial dimension. The subsystems are then coupled at the positions of the δ -wells $x = \pm b$. The depth of the potentials is controlled by V_0^D . Both the depth V_0^D and the distance $2b$ between the wells correspond to the coupling parameter v in the matrix model. The coupling strength between the two subsystems is controlled by γ and is only present at the two points $x = \pm b$, i.e. the potential has no spatial extension. The dimensionless coupled Gross-Pitaevskii equations read

$$\begin{aligned} \left[-\frac{\partial^2}{\partial x^2} - g|\psi_A|^2 + V_0^D(\delta(x-b) + \delta(x+b)) \right] \psi_A \\ + i\gamma [\delta(x-b)\psi_B(b) - \delta(x+b)\psi_B(-b)] = \mu_A \psi_A, \\ \left[-\frac{\partial^2}{\partial x^2} - g|\psi_B|^2 + V_0^D(\delta(x-b) + \delta(x+b)) \right] \psi_B \\ - i\gamma [\delta(x-b)\psi_A(b) - \delta(x+b)\psi_A(-b)] = \mu_B \psi_B, \end{aligned} \quad (14)$$

with the same physical interpretation of μ_A and μ_B as in (11) for the matrix model. Stationary states of the system are calculated numerically exact by integrating the wave functions outward from $x = 0$ and by imposing the appropriate boundary conditions on the wave functions. We require that the wave functions have to approach zero when $x \rightarrow \pm\infty$. For numerical purposes it is sufficient for the wave functions to have small values at $x = \pm x_{\text{max}}$,

$$\psi_{A,B}(\pm x_{\text{max}}) \approx 0. \quad (15)$$

An additional condition can be required for the norm of the wave function. In agreement with the normalized ansatz (13) in the matrix model we search for solutions that fulfill

$$||\psi_{A,B}||^2 = 1. \quad (16)$$

Both wave functions are real at $x = 0$. With this we enforce a global phase and the phase difference between the two modes at $x = 0$ to be $\varphi_{\text{rel}} = 0$.

The 10 (real) free parameters are $\text{Re } \mu_{A,B}$, $\text{Im } \mu_{A,B}$, $\text{Re } \psi_{A,B}(0)$, $\text{Re } \psi'_{A,B}(0)$ and $\text{Im } \psi'_{A,B}(0)$. They are chosen such that the 10 (real) conditions, i.e. the norm (16) and the boundary conditions at $x = \pm x_{\text{max}}$ (15) are fulfilled. Note that there are no constraints on the $\mu_{A,B}$. We will see that for stationary \mathcal{PT} -symmetric solutions the result is $\mu_A = \mu_B \in \mathbb{R}$. This is not a constraint on the root search.

2.3. Model with a spatial resolution of both the potential well and the coupling

We consider an additional system and remove a further restriction, viz. the point-like coupling approach, by duplicating the system from (6), where the wells are formed by a harmonic trap and divided by a Gaussian potential barrier. This does not only provide us with a system with much more realistic potential wells but also allows us to extend the coupling of the two subsystems over the whole space. The time-independent GPEs of the system read

$$\begin{aligned} \left(-\frac{\partial^2}{\partial x^2} - g|\psi_A|^2 + \frac{1}{4}x^2 + V_0^G e^{-\sigma x^2} \right) \psi_A + i\gamma x e^{-\rho x^2} \psi_B &= \mu_A \psi_A, \\ \left(-\frac{\partial^2}{\partial x^2} - \underbrace{g|\psi_B|^2}_{\text{contact}} + \underbrace{\frac{1}{4}x^2 + V_0^G e^{-\sigma x^2}}_{\text{trap}} \right) \psi_B - \underbrace{i\gamma x e^{-\rho x^2} \psi_A}_{\text{coupling}} &= \mu_B \psi_B. \end{aligned} \quad (17)$$

The parameter V_0^G controls the height of the potential barrier between the two wells in one subsystem and together with the width σ of the barrier it relates to the coupling strength v in the matrix model. Again the coupling between the two subsystems is controlled by a parameter labelled γ .

To solve this equation we use an ansatz of coupled Gaussian functions (compare [52, 53]),

$$\psi = \sum_{\substack{i=A,B \\ j=1,2}} \psi_{i,j} = \sum_{\substack{i=A,B \\ j=1,2}} \exp(a_{i,j}x^2 + b_{i,j}x + c_{i,j}). \quad (18)$$

We use four wave functions, two for each subsystem ($i = A, B$) and place one in each well ($j = 1, 2$). Again we place restrictions on our ansatz. We require that the norm of each subsystem is one, which reduces our parameter set by two. In addition we require

$$\begin{aligned} \text{Im } c_{A,1} &= \varphi_A, & \text{Im } c_{B,1} &= \varphi_B + \varphi_{\text{rel}}, \\ \text{Im } c_{A,2} &= -\varphi_A, & \text{Im } c_{B,2} &= -\varphi_B + \varphi_{\text{rel}} \end{aligned} \quad (19)$$

with a constant φ_{rel} determining the phase difference between the two modes, and again reducing the parameter set by two. Therefore from the 24 parameters $a_{i,j}, b_{i,j}, c_{i,j} \in \mathbb{C}$ 20 free parameters remain and must be determined such that adequate solutions are

found. With these constraints the ansatz is consistent with the ansatz for the matrix model and the system with the double- δ potential.

To obtain solutions of (17) we apply the time-dependent variational principle [54] to the time-dependent GPEs

$$\begin{aligned} \left(-\frac{\partial^2}{\partial x^2} - g|\psi_A|^2 + \frac{1}{4}x^2 + V_0^G e^{-\sigma x^2} \right) \psi_A + i\gamma x e^{-\rho x^2} \psi_B &= i\frac{\partial}{\partial t} \psi_A, \\ \left(-\frac{\partial^2}{\partial x^2} - \underbrace{g|\psi_B|^2}_{\text{contact}} + \underbrace{\frac{1}{4}x^2 + V_0^G e^{-\sigma x^2}}_{\text{trap}} \right) \psi_B - \underbrace{i\gamma x e^{-\rho x^2} \psi_A}_{\text{coupling}} &= i\frac{\partial}{\partial t} \psi_B. \end{aligned} \quad (20)$$

We search a parameter set for our ansatz, which minimizes the difference between the left-hand and right-hand side of the equation, viz. we determine the minimum of the functional

$$I = \|H\psi - i\dot{\psi}\|^2. \quad (21)$$

In this procedure $\psi(t)$ is kept constant for a given point in time and $\dot{\psi} = \phi$ is varied to minimize I . Since the wave function $\psi(z(t))$ is not varied we require that the parameters $z = \{a_{i,j}, b_{i,j}, c_{i,j}\}$ do not change. A variation with respect to \dot{z} leads to the equations of motion for the variational parameters, which follow from

$$\left\langle \frac{\partial \psi}{\partial z} \left| \dot{\psi} - iH\psi \right. \right\rangle = 0. \quad (22)$$

A more elaborate explanation of the method can be found in [43]. With a numerical root search we can now determine those states which satisfy the 20 conditions

$$0 = \dot{a}_{i,j}, 0 = \dot{b}_{i,j}, \quad (23)$$

$$\mu_i = i\dot{c}_{i,1}^* = i\dot{c}_{i,2}^* \Rightarrow 0 = \dot{c}_{i,1} - \dot{c}_{i,2} \text{ with } i = A, B. \quad (24)$$

For \mathcal{PT} -symmetric solutions the chemical potentials of the subsystems will fulfil $\mu_A = \mu_B \in \mathbb{R}$.

3. \mathcal{PT} -symmetric properties and bifurcation structure of the systems

First we will examine analytical solutions of the matrix model. The bifurcation structure of these solutions and their \mathcal{PT} -symmetric properties will be discussed. Furthermore the differences and similarities between this four-dimensional hermitian matrix model and the two-dimensional matrix model with imaginary potential will be examined.

In a next step the results obtained with the matrix model will be compared with the spatially extended models. Also the influence of the phase difference between the two modes will be investigated.

3.1. Bifurcations structure and \mathcal{PT} -symmetric properties of the matrix model

To obtain analytical solutions we have to impose some constraints on the ansatz of the wave function of the matrix model (11). \mathcal{PT} -symmetric solutions must fulfil the

condition (2) which for this matrix model results in

$$\psi_{j,1} = \psi_{j,2}^* \quad \text{with } j = A, B \quad (25)$$

and

$$\psi_{A,i} = \psi_{B,i}^* \quad \text{with } i = 1, 2. \quad (26)$$

This ensures that the particle loss in one system is compensated by the other. These restrictions lead to the ansatz

$$\psi = \frac{1}{\sqrt{2}} (e^{i\varphi}, e^{-i\varphi}, e^{-i\varphi}, e^{i\varphi}) \quad (27)$$

with which we obtain an analytical expression for the chemical potentials of two \mathcal{PT} -symmetric solutions

$$\mu = -\frac{g}{2} \pm \sqrt{v^2 + \gamma^2}. \quad (28)$$

A more detailed calculation is given in Appendix B.

The solutions are plotted in figure 3 and labelled s_1 and s_2 . For different values of g the solutions are shifted up or down. For increasing values of γ the difference of the values of the chemical potential of the two states is increased.

\mathcal{PT} -broken states do not need to obey condition (25) but (26) still must be fulfilled since the influx and outflux between subsystem A and B must be equal. Therefore the ansatz for these states reads

$$\psi = (\cos \theta e^{i\varphi}, \sin \theta e^{-i\varphi}, \cos \theta e^{-i\varphi}, \sin \theta e^{i\varphi}) \quad (29)$$

with $\mu_A = \mu_B^*$. The calculation in Appendix B yields the analytical expressions for the chemical potentials

$$\mu_A = \mu_B^* = -\frac{g}{2} \left(2 \mp \sqrt{P + \frac{\gamma^2}{v^2} P^2} - P \right) \quad \text{with } P = \frac{1}{2} \pm \frac{\sqrt{g^2 + 16\gamma^2}}{2g}. \quad (30)$$

Note that the \mp and \pm are independent and we therefore obtain four expressions (30) for \mathcal{PT} -broken states. However two of these solutions only exist in an analytically continued system (see figure 3).

For $|g| < 2v$ the state s_2 passes through a pitchfork bifurcation at

$$\gamma_c = \sqrt{\frac{4v^4}{g^2} - v^2}, \quad (31)$$

in which a_1 and a_2 are created. For $\gamma > \gamma_c$ these two states have the same $\text{Re } \mu_A$ but a complex conjugate $\text{Im } \mu_A$. This means that one of the states gains particles in subsystem A while in subsystem B it is depleted, and vice versa. The pitchfork bifurcation occurs at smaller values of γ_c for an increasing nonlinearity g until for $|g| = 2v$ the value of γ_c reaches zero. For values of $|g| > 2v$ the bifurcation between $a_{1,2}$ and s_2 no longer occurs and the states $a_{1,2}$ exist independent of s_2 for all γ . For $g < 0$ the bifurcation occurs not with the state s_2 but with s_1 . Thus we have shown that \mathcal{PT} -symmetric states exist for the closed four-dimensional hermitian matrix model and \mathcal{PT} -symmetry breaking can be observed.

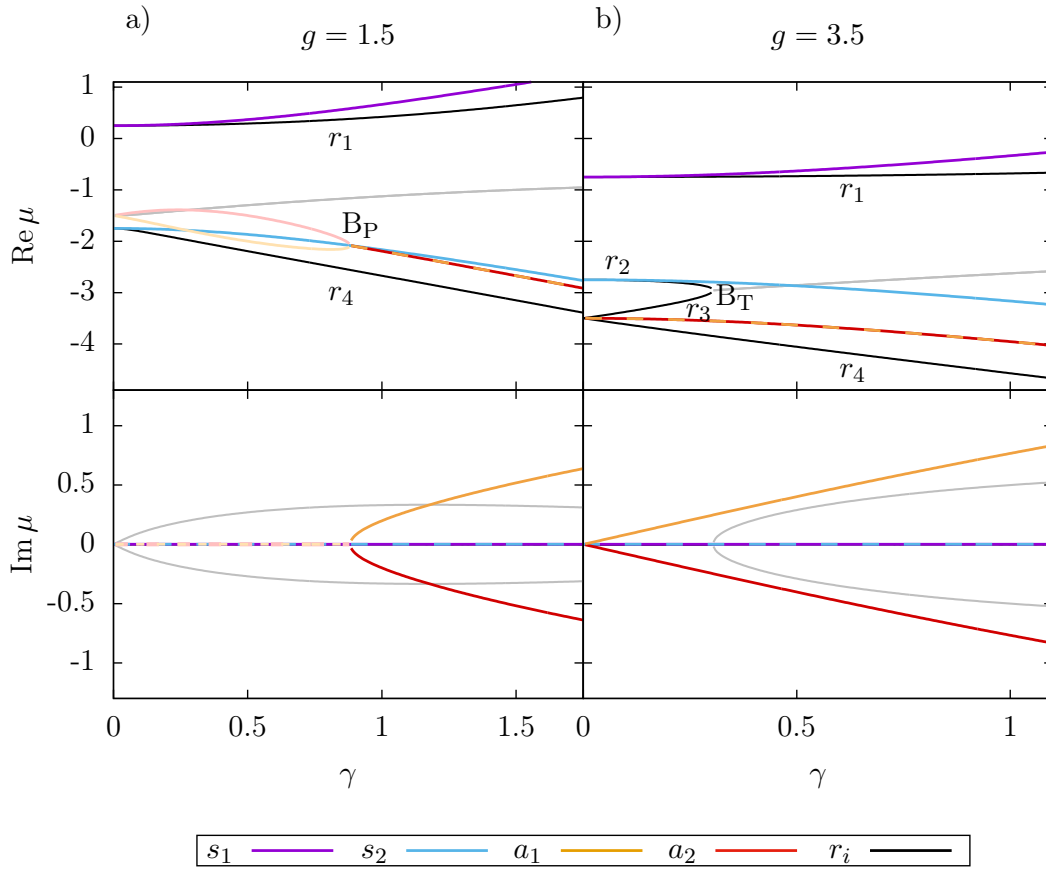


Figure 3. Analytical solutions for the chemical potential of (10) are shown. The \mathcal{PT} -symmetric states are denoted by s_1 and s_2 . \mathcal{PT} -broken states are labelled with a_1 and a_2 . Solutions of the effective system (33) are labelled with r_i . The states r_2 and r_3 only exist for $|g| > 2$ and therefore appear only in figure b. The coupling strength is set to $v = 1$. In a) the nonlinearity is set to $g = 1.5$ while in b) it is set to $g = 3.5$. The pitchfork bifurcation between the states $a_{1,2}$ and s_2 in a) is labelled with B_P and occurs at $\gamma \approx 0.882$. The tangent bifurcation between states r_2 and r_3 in b) is marked by B_T . The analytically continued solutions are plotted using lighter colours.

Besides these states there is another class of states in the four-dimensional matrix model. Wave functions which fulfil the condition

$$\psi_{A,i} = -i\psi_{B,i} \text{ with } i = 1, 2 \text{ and } \psi_{A,i}, i\psi_{B,i} \in \mathbb{R} \quad (32)$$

lead to decoupled equations for ψ_A and ψ_B and result in the effective two-dimensional model

$$\begin{pmatrix} -g|\psi_1|^2 - \gamma & v \\ v & -g|\psi_2|^2 + \gamma \end{pmatrix} \begin{pmatrix} \psi_1 \\ \psi_2 \end{pmatrix} = \mu \begin{pmatrix} \psi_1 \\ \psi_2 \end{pmatrix} \text{ and } \psi_{1,2} \in \mathbb{R}. \quad (33)$$

These states effectively describe a double-well system with a real potential, where one potential well is lowered and the other is raised by the value of γ . As expected we find that the amplitude of the wave function in the higher well is lower than in the other. For $\gamma = 0$ the system crosses over to a symmetric double-well model with no coupling

and therefore we can see in figure 3a that the state r_1 merges with the state s_1 and the state r_4 merges with the state s_2 . For values $g > 2v$ the bifurcation between the \mathcal{PT} -symmetric and \mathcal{PT} -broken states no longer exists and two new states r_2 and r_3 emerge. Now at $\gamma = 0$ the states r_1 and s_1 as well as r_2 and s_2 become equal. Also r_3 , r_4 and s_4 merge. For increasing γ the states r_2 and r_3 vanish in a tangent bifurcation. The method used to solve (33) is described in Appendix B.

We can compare the results of the four-dimensional matrix model in figure 3 with those of the two-dimensional matrix model shown in figure 1. It is immediately clear that our system shows a new and richer bifurcation scenario which differs from the two-dimensional matrix model. While the \mathcal{PT} -symmetric eigenvalues of the states in the two-dimensional system approach each other for increasing coupling strengths γ until they merge in a tangent bifurcation, in our system the eigenvalues increase in distance for larger values of γ and no bifurcation between the two states $s_{1,2}$ occurs. However, some generic features remain the same. In both cases the \mathcal{PT} -symmetric state s_2 with a real μ passes through a pitchfork bifurcation, out of which the \mathcal{PT} -broken states with complex μ emerge. For both models this bifurcation moves to smaller values of γ until, for a critical value of the nonlinearity g , the bifurcation vanishes and the \mathcal{PT} -symmetric and \mathcal{PT} -broken states never coincide.

One advantage of using a matrix model compared to systems with a more realistic spatially extended description is that the matrix model gives an overview over all possible effects in a system while remaining straightforward to calculate. Also the knowledge about symmetry properties and existence of states gained from the matrix model can help finding states in the more complicated models, e.g. by choosing appropriate initial values for a root search. Since we want to concentrate our investigation on the \mathcal{PT} -symmetric properties of the subsystems, we will not further investigate the states r_i .

3.2. Comparison of the matrix model and the model with a spatial resolution of the wave function

The results of the system with the double- δ potentials are given in figure 4 in comparison with those of the matrix model. To be able to compare the two models the parameters in the matrix model are replaced by $g \rightarrow g/g_0$ and $\gamma \rightarrow \gamma/\gamma_0$. Also a shift $\Delta\mu$ in the chemical potential is introduced. Then the parameters γ_0 , g_0 , v and $\Delta\mu$ are fitted to the results of the double- δ model. How these parameters are connected to the extended model can be seen in Appendix C.

In contrast to the matrix model the double- δ system includes spatial properties of the wave functions. In figure 5 the wave functions for the parameters marked in figure 4 are shown. One can clearly observe the non-differentiability of the wave functions at the locations $x = \pm b$ of the δ -potentials. It is also clearly visible that the states with complex chemical potential are \mathcal{PT} -broken (see figure 5c). The two wave functions for the subsystems A and B fulfil the condition $\psi_A(x) = \psi_B^*(x)$ which ensures that the loss and gain in each subsystem is balanced by the gain and loss in the other subsystem

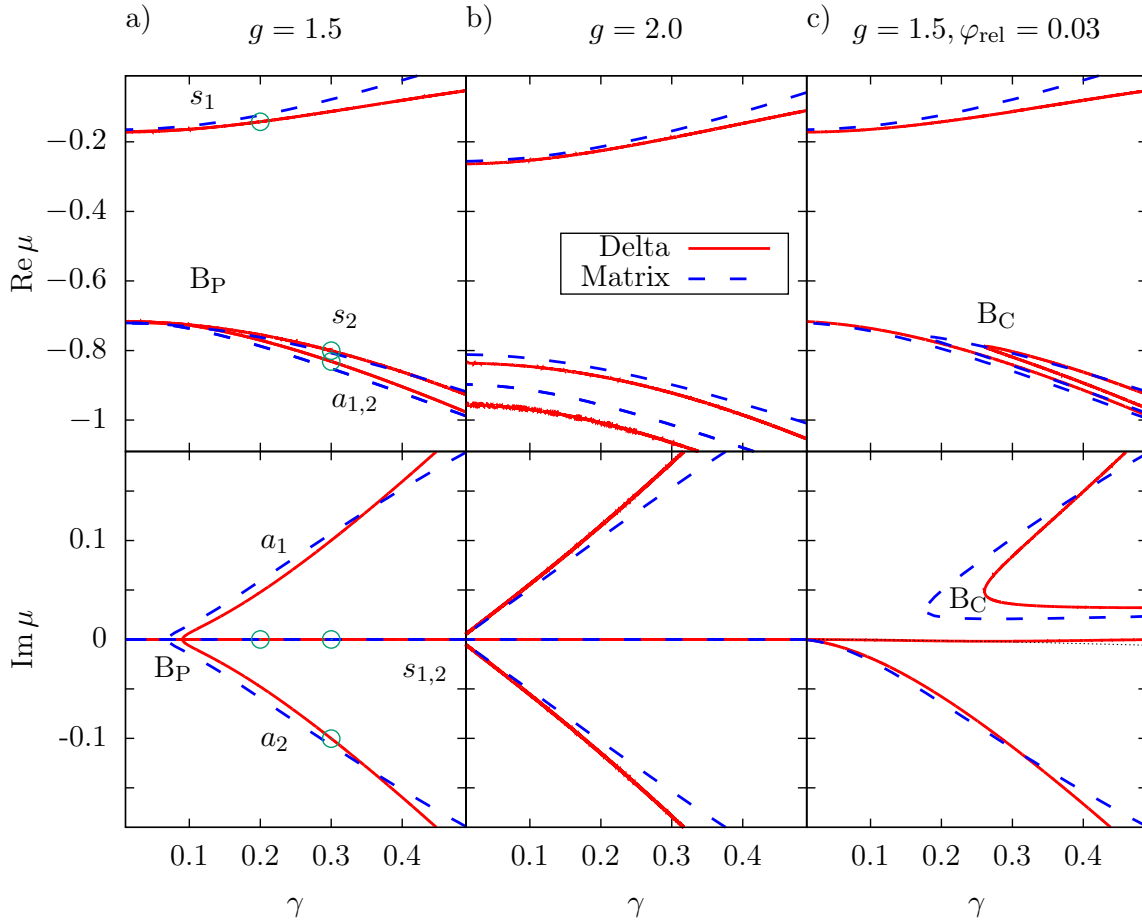


Figure 4. Chemical potential $\mu = \mu_A = \mu_B^*$ for the matrix model (11) (blue dashed lines). The parameters of the matrix used for all three plots are $g_0 = 2.75$, $v = 0.28$ and $\gamma_0 = 1.27$. The shift of the chemical potential of the matrix model is $\Delta\mu = -0.17$. For both figures a) and b) the phase difference φ_{rel} was set to zero. Figure a) was calculated for a nonlinearity of $g = 1.5$. The different states are denoted by $s_{1,2}$, $a_{1,2}$. In plot b) a nonlinearity of $g = 2.0$ was used. For plot c) the same nonlinearity as in plot a) was used but the phase difference was set to $\varphi_{\text{rel}} = 0.03$. The figure also contains the results for the double- δ -system (red solid lines). For the coupling of the two subsystems V_0^D was set to 1.0 and the δ -potentials were located at $b = \pm 1.1$. The same nonlinearities as for the matrix model were used. In figure a) the parameters for which the wave functions are shown in figure 5 are marked by green circles. A pitchfork bifurcation between the states s_2 and $a_{1,2}$ is denoted by B_P . An additional cusp bifurcation appearing in the case φ_{rel} is marked by B_C .

and the \mathcal{PT} -symmetry of the potential is maintained. Furthermore the wave function of the ground state (figure 5a) is much more localized in the potential wells than the wave function of the excited state (figure 5b).

When we compare the solutions of the matrix model with those of the model with the double- δ potential we observe that the qualitative bifurcation structure of the states is the same for both models but some quantitative deviations can be seen. Before we continue our investigation of the cause of these differences in section 3.3 we will take a

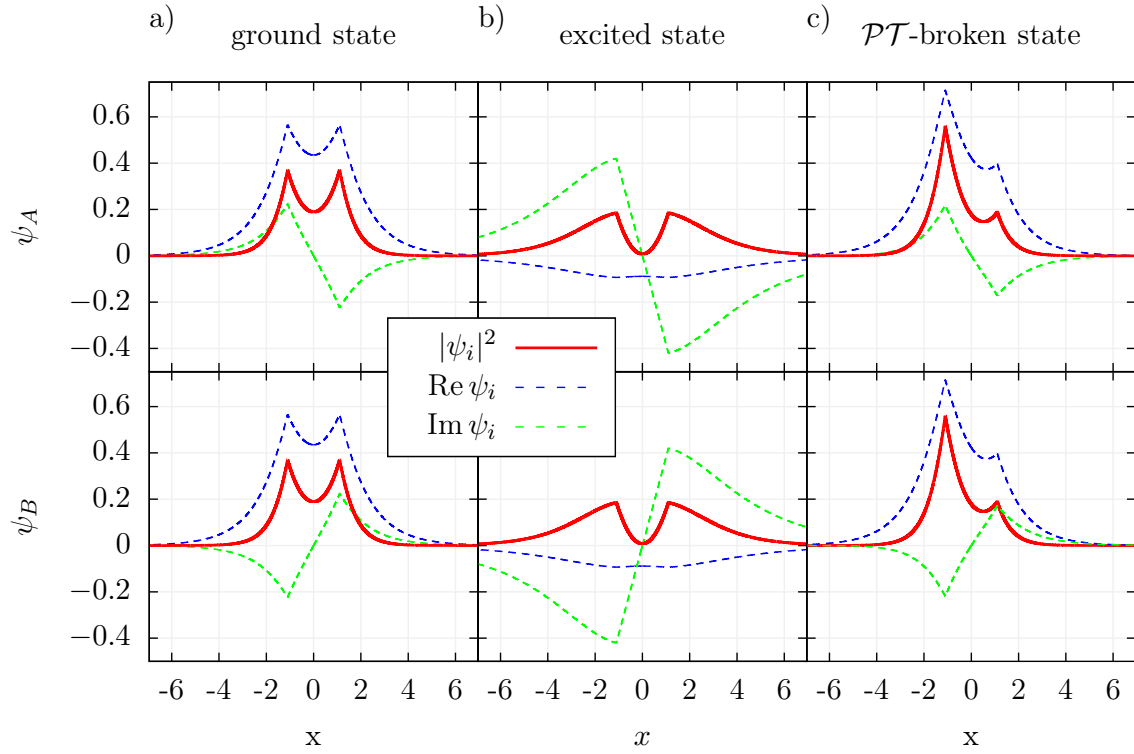


Figure 5. Wave functions of the double- δ potential system for the parameter sets marked in figure 4a. a) Wave function of the \mathcal{PT} -symmetric ground state. b) Wave function of the \mathcal{PT} -symmetric excited state. In c) the broken symmetry of the \mathcal{PT} -broken state can be recognized.

look at the influence of the phase difference φ_{rel} between the two subsystems.

To examine the influence of the phase difference on the bifurcation scenario we show in figure 4c the case in which the phase difference between the subsystems is set to $\varphi_{\text{rel}} = 0.03$. The pitchfork bifurcation B_P in figure 4c turns into a cusp bifurcation B_C . While the central (\mathcal{PT} -symmetric) state s_1 exists on both sides of the bifurcation point, the two outer (\mathcal{PT} -broken) states $a_{1,2}$ are created in the bifurcation of figure 4a. In the cusp bifurcation of figure 4c one of the outer states (depending on the sign of φ_{rel}) merges with the central state and the other outer state performs a continuous transition to the central state for smaller values of γ . Also the \mathcal{PT} -symmetry of all states is broken. The asymmetry increases for the central state for increasing values of φ_{rel} .

If we introduce the phase difference $\exp(i\varphi_{\text{rel}})$ between the two subsystems explicitly into the stationary GPE (13) for the matrix model, we obtain for the subsystem A

$$\begin{aligned} \mu_A \psi_{A,1} &= -g|\psi_{A,1}|^2 \psi_{A,2} + v\psi_{A,2} + \sin(\varphi_{\text{rel}})\gamma\psi_{B,1} - i\cos(\varphi_{\text{rel}})\gamma\psi_{B,1}, \\ \mu_A \psi_{A,1} &= -g|\psi_{A,1}|^2 \psi_{A,2} + v\psi_{A,1} - \underbrace{\sin(\varphi_{\text{rel}})\gamma\psi_{B,2}}_{\text{asym. pot.}} + \underbrace{i\cos(\varphi_{\text{rel}})\gamma\psi_{B,2}}_{\text{gain or loss}}. \end{aligned} \quad (34)$$

We see that a phase difference between the two subsystems leads to different contributions to the real and imaginary part of the effective potential of each subsystem.

The real part of the effective potential can therefore become asymmetric (this not only depends on the phase difference φ_{rel} but also on the phase value of the wave function in the other subsystem).

The influence of an asymmetric double-well potential on the bifurcation structure has been discussed previously [55]. For an asymmetric potential there is no longer a pitchfork bifurcation but a tangent bifurcation. We can compare this to the well known normal forms of the two parameter bifurcation theory [56]. The normal form of the cusp bifurcation is

$$0 = \dot{x} = f_C(x) = \beta + \alpha x - x^3, \quad (35)$$

with the bifurcation parameters α and β . In our model the role of the second parameter β is taken by the phase difference φ_{rel} between the two subsystems. A constant $\varphi_{\text{rel}} = 0$ (which is equivalent with $\beta = 0$) defines a line in the $\varphi_{\text{rel}}\text{-}\gamma$ parameter space. On this line the pitchfork bifurcation scenario emerges.

We have seen that the phase difference between the two modes is critical to obtain a \mathcal{PT} -symmetric system, and the breaking of this symmetry changes the bifurcation structure. Only for $\varphi_{\text{rel}} = 0$ \mathcal{PT} -symmetric states are observed.

3.3. Comparison of the models and usefulness of the matrix model

In the system (17) the two modes are coupled over a spatially extended range and therefore the continuous change of the phase in the wave functions may play a role. In figure 6 we show the stationary states of the matrix model (10) in comparison with those of the smooth potential system (17). The parameters of the matrix model (g_0, γ_0 and v) and a shift of the chemical potential $\Delta\mu$ were adjusted to the solution of the model (17) but remained the same for all calculations in figure 6 with different values for g and φ_{rel} . In Appendix C it is shown how the discrete matrix model can be derived from a continuous model.

Again we see a pitchfork bifurcation (figure 6a) in the lower state which, for increasing values of the nonlinearity g , moves to smaller values of γ . The two new states created in this bifurcation are non-stationary ($\mu_{A,B} \notin \mathbb{R}$) \mathcal{PT} -broken states. By further increasing g the value of γ at which the bifurcation occurs moves to even smaller values of γ until it reaches $\gamma = 0$. Thus the qualitative behaviour is exactly the same as in the two previously investigated models. It is generic for the coupled double-well structure. If the phase between the two subsystems is changed to a non-zero value, the pitchfork bifurcation from figure 6a changes into a cusp bifurcation (compare figure 6c). This is the same behaviour as observed in figure 4 for the double- δ -potential. No change of the bifurcation structure or the \mathcal{PT} -symmetric properties due to the extended coupling is observed. However, as can be seen in figure 6a-c the agreement with the matrix model is nearly perfect and much better than the agreement between the matrix model and the model with the δ -potential wells.

Taking a closer look at the states of the matrix model one discovers that the upper and lower states are symmetric with respect to $-g/2$ as can be seen in (28). This is no

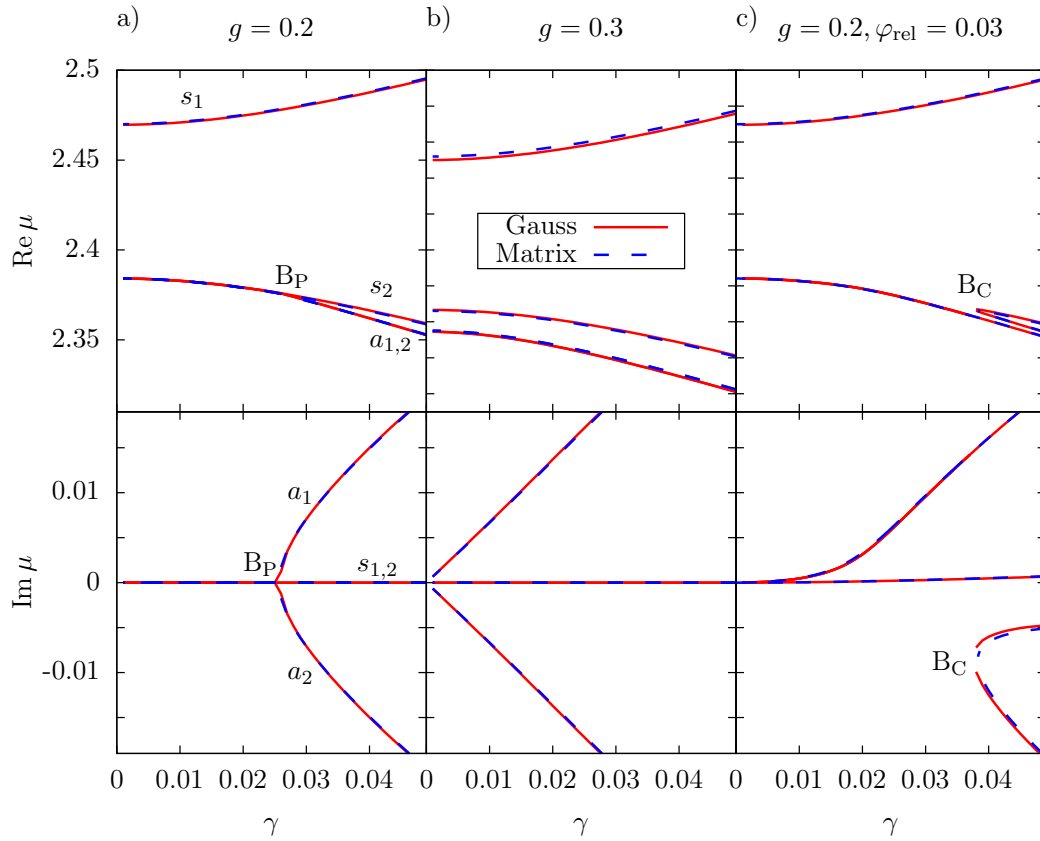


Figure 6. Comparison of the eigenvalues of the matrix model from (10) (blue dashed lines) with the eigenvalues of the system (17) (red solid lines), in which the BEC is trapped in a smooth harmonic potential separated into two wells by a Gaussian potential barrier. The fit parameters for the matrix model are $g_0 = 2.78$, $v = 0.043$ and $\gamma_0 = 0.92$ and are used for all cases a)-c). The chemical potential of the matrix model is shifted by $\Delta\mu = 2.463$. The height of the Gaussian potential barrier in system (17) is $V_0^G = 0.25$ with the width $\sigma = 0.5$. Figures a) and c) contain the results for $g = 0.2$, while figure b) is plotted for $g = 0.3$. In figure c) the phase difference is non-zero ($\varphi_{\text{rel}} = 0.03$).

longer true for the models with a spatial description. To make this asymmetry visible we examine figure 7 in which one state is mirrored onto the other, e.g. for one state

$$\mu_{\text{mirror}} = \mu_0 - \mu \quad (36)$$

is plotted and μ_0 is the average value of the chemical potential of both states at $\gamma = 0$. One observes that the deviation is much more pronounced in the model with δ -wells than in the smooth potential from (17).

In the comparison of the fit parameters g_0 , v and γ_0 (see table 1), one parameter with vastly different values is evident. The coupling strength v of the two potential wells in the δ -potential model case is approximately 6.5 times larger than in the case of the harmonic trap with the potential well. This means that the separation of the two wells is much less pronounced due to shallower wells in the case of the δ -potential. This leads to wave functions which are not as localized as in the case of the smooth potential.

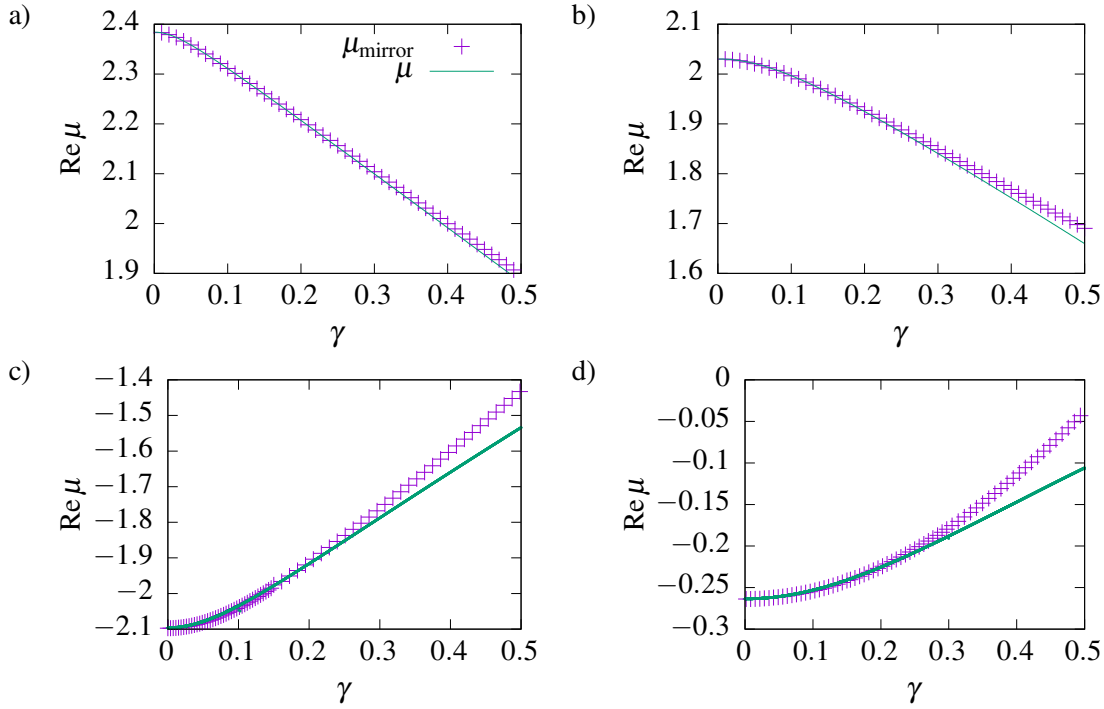


Figure 7. Ground state and mirrored excited state ($\mu_{\text{mirror}} = \mu_0 - \mu$). The states are not symmetric. Figures a) and b) show the results for the Gaussian model (17) with $g = 0.2$ and $\mu_0 = 4.854$ and $\mu_0 = 4.2733$, respectively. Figures c) and d) show the results of the double- δ model (14) with $g = 2.0$ and $\mu_0 = -4.5$ and $\mu_0 = -1.1$, respectively. In the Gaussian model the height of the potential barrier between the two wells in each subsystem is changed. For a) the barrier height is $V_0^G = 4.0$, for b) it is $V_0^G = 2.5$. In the case of the δ -model the (real) depth of the potentials is lowered from $V_0^D = 1.0$ in a) to $V_0^D = 2.5$ in b).

Table 1. Fit parameters of the matrix model used for the comparison with the spatially extended models in figures 4 and 6.

Comparison with	g_0	v	γ_0	$\Delta\mu$	V_0^G	σ	V_0^D	b
double- δ model	2.75	0.28	1.27	-0.17	—	—	1.0	1.1
smooth potential	2.78	0.043	0.92	2.463	2.5	0.5	—	—

Therefore the contribution of the overlap of the wave functions, which was negligible for the smooth potential, increases. The matrix model is not capable of describing the nonlinear interaction between wave functions of different modes. Only the nonlinear scattering process in the same well is taken into account.

For further investigation one can increase the distance between the wells or deepen them. One might expect that the stationary states then would be in a better agreement with the matrix model. We compare the model with smooth potentials for different barrier heights (figure 7a and figure 7b). For a lower potential barrier the asymmetry of the two states becomes more pronounced. The same is true for the δ -model (figure 7c and figure 7d).

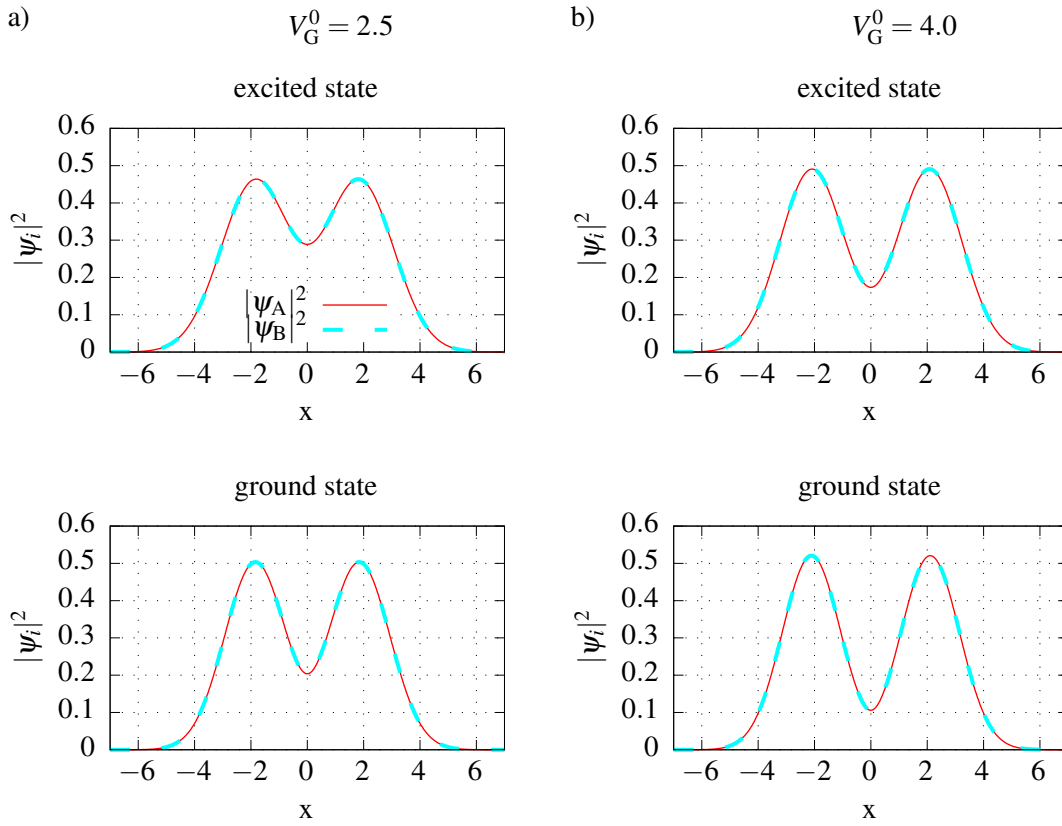


Figure 8. Wave functions for the ground and excited states in the Gaussian model for different potential barriers (in a) $V_0^G = 2.5$, in b) $V_0^G = 4.0$) for a nonlinearity of $g = 0.2$. The overlap of the Gaussians at $x = 0$ is much higher for the lower potential barrier in a) and for the excited states.

The wave functions for the different parameter sets are shown in figure 8. Here the probability density of the ground and excited state for the smooth potential model with different heights for the potential barrier can be seen. One observes a higher probability density in the overlap region around $x = 0$ for the excited states. This overlap increases for a lower potential barrier. Thus, we can conclude that the matrix model captures all relevant information of the bifurcation scenario and the \mathcal{PT} -symmetric properties as long as the different potential wells are sufficiently separated. A larger overlap leads to quantitative changes and the loss of a mirror symmetry of pairs of values for the chemical potential in the (μ, γ) -diagram, however, it does not affect the generic structure of the states.

4. Summary and Outlook

For an experimental realization of a \mathcal{PT} -symmetric double-well potential the description of a physical environment which implements the gain and loss of a complex potential is an important prerequisite. By combining two double-well subsystems into one closed hermitian system we have found such a realization.

For the four-dimensional matrix model without a phase difference between the two subsystems analytical solutions for all \mathcal{PT} -symmetric and \mathcal{PT} -broken states were found. Although the four-dimensional matrix model showed a new and different bifurcation scenario in comparison with the two-dimensional matrix model from [27] some generic features remained the same.

The matrix model showed the same qualitative bifurcation scenario as the two spatially extended models. Deviations could be observed when the two wells of the systems were not isolated enough such that the wave functions in each well had a significant overlap between the wells. In this case the solutions from the systems with a spatially resolved wave function differed from those of the matrix model. A larger overlap leads to quantitative changes and the loss of a mirror symmetry of pairs of energy eigenvalues in the (μ, γ) -diagram, however, it does not affect the generic structure of the states.

The influence of the phase difference between the two subsystems was also examined. While the coupling strength γ between the two subsystems took the role of one bifurcation parameter, the phase difference φ_{rel} took the role of another, leading to a two-parametric cusp bifurcation. This bifurcation degenerated for $\varphi_{\text{rel}} = 0$ into a pitchfork bifurcation. Only in this case \mathcal{PT} -symmetric states could be observed which makes the phase difference between the subsystems critical for the \mathcal{PT} -symmetric properties of the system.

The matrix model can be investigated further. Under the assumption that the two wells of the system are sufficiently isolated the matrix model reduces the description of the system to a low number of key parameters. Therefore the analytically accessible matrix model of this paper could be helpful to gain more insight into the behaviour of coupled BECs. In particular a similar approach to realize a \mathcal{PT} -symmetric quantum system via the coupling of two condensate wave functions was studied in [47] and revealed complicated stability properties. This system should also be representable in our four-mode description such that analytic expressions should be obtainable.

Acknowledgments

This work was supported by Deutsche Forschungsgemeinschaft.

Appendix A. Time-independent solutions of the nonlinear GPE

We will first consider a linear GPE in appropriate units

$$i\frac{\partial}{\partial t}\psi = -\Delta\psi + V(x)\psi. \quad (\text{A.1})$$

To find time-independent solutions one uses

$$\psi(t) = \psi_0 \exp(-i\mu t) \quad (\text{A.2})$$

which leads to the time-independent equation

$$\mu\psi_0 = -\Delta\psi_0 + V(x)\psi_0. \quad (\text{A.3})$$

Solutions with a real μ are true stationary states, i.e. only the global phase is changed with $\exp(-i \operatorname{Re} \mu t)$. By contrast states with a complex μ , in addition to the phase change, increase or decrease in the probability amplitude exponentially with $\exp(\operatorname{Im} \mu t)$.

For a GPE with a nonlinearity this is no longer true. If we consider

$$i \frac{\partial}{\partial t} \psi = -\Delta \psi + V(x) \psi + g |\psi|^2 \psi \quad (\text{A.4})$$

the previous ansatz (A.2) will lead to

$$\mu \psi_0 = -\Delta \psi_0 + V(x) \psi_0 + g |\psi_0|^2 \psi_0 \exp(-2i \operatorname{Im} \mu t). \quad (\text{A.5})$$

Also in this case, if μ is a purely real number, the states ψ are stationary. But for states with a chemical potential μ which has an imaginary part $\operatorname{Im} \mu \neq 0$ the interpretation changes. In the nonlinear case (A.2) is only a solution in the limit $t \rightarrow 0$. Therefore for small times the probability amplitude of these states still approximatively increases or decreases exponentially, but the true time evolution deviates from this linear solution as time increases.

Appendix B. Analytical solutions of the matrix model

We want to show how to calculate the analytical solution for the four dimensional matrix model in (11). As an ansatz for \mathcal{PT} -symmetric solutions (27) is used. We obtain the equations

$$\begin{aligned} -\frac{g}{2} + v e^{-2i\varphi} - i\gamma e^{-2i\varphi} &= \mu, \\ -\frac{g}{2} + v e^{2i\varphi} + i\gamma e^{2i\varphi} &= \mu. \end{aligned} \quad (\text{B.1})$$

With the substitution $x = \exp(2i\varphi)$ we can transform these equations into

$$\begin{aligned} (v - i\gamma) \frac{1}{x} &= \mu + \frac{g}{2}, \\ (v + i\gamma) x &= \mu + \frac{g}{2}. \end{aligned} \quad (\text{B.2})$$

This in turn leads to

$$(v - i\gamma) \frac{1}{x} = (v + i\gamma) x \quad (\text{B.3})$$

and therefore we obtain

$$x = \pm \sqrt{\frac{v - i\gamma}{v + i\gamma}}, \quad (\text{B.4})$$

which can be inserted into one of the equations in (B.1) and yields to the two \mathcal{PT} -symmetric solutions

$$\mu = -\frac{g}{2} \pm \sqrt{v^2 + \gamma^2}. \quad (\text{B.5})$$

For the \mathcal{PT} -broken solutions the ansatz (29) is used and results in

$$\begin{aligned} -g \cos^2 \theta + v \tan \theta e^{-2i\varphi} - i\gamma e^{-2i\varphi} &= \mu, \\ -g \sin^2 \theta + v \cot \theta e^{2i\varphi} + i\gamma e^{2i\varphi} &= \mu. \end{aligned} \quad (\text{B.6})$$

By eliminating μ and separating the equation into its real and imaginary part the equation system

$$\begin{aligned} -g(\cos^2 \theta - \sin^2 \theta) + v(\tan \theta - \cot \theta) \cos 2\varphi &= 0 \\ -v(\tan \theta + \cot \theta) \sin 2\varphi - 2\gamma \cos 2\varphi &= 0 \end{aligned} \quad (\text{B.7})$$

remains, which can be transformed into

$$\sin 2\theta = -\frac{2v}{g} \cos 2\varphi = -\frac{v}{\gamma} \tan 2\varphi. \quad (\text{B.8})$$

By the substitution $x = \exp(2i\varphi)$ the quasi palindromic polynomial

$$x^4 - 2Ax^3 + 2x^2 + 2Ax + 1 = 0 \quad \text{with } A = -i\frac{g}{2\gamma} \quad (\text{B.9})$$

is obtained. The four solutions of this polynomial are

$$x = \frac{1}{2}(z \pm \sqrt{4 + z^2}) \quad \text{with } z = A \pm \sqrt{A^2 - 4} = -\frac{gi}{\gamma}P \quad \text{with } P = \frac{1}{2} \pm \frac{\sqrt{g^2 + 16\gamma^2}}{2g}. \quad (\text{B.10})$$

Note that the \pm for x and P are independent and therefore lead to four solutions. By inserting the solutions into one of the equations in (B.6) one obtains the analytical expressions for the chemical potential,

$$\mu = -\frac{g}{2} \left(2 \mp \sqrt{P + \frac{\gamma^2}{v^2}P^2 - P} \right). \quad (\text{B.11})$$

Note that without an analytical continuation of the equations the parameters θ and φ in the ansatz of the wave functions must be real. Therefore one can see that two of the solutions for the chemical potential have complex θ or φ over the whole parameter range and therefore are shown in lighter colours in figure 3. The other two solutions exist if the constraint

$$\gamma > \gamma_c = \sqrt{\frac{4v^4}{g^2} - v^4} \quad (\text{B.12})$$

is fulfilled.

For the effective matrix model in (33) with the ansatz

$$\psi = (\cos \theta, \sin \theta) \quad (\text{B.13})$$

one obtains the equations

$$\begin{aligned} -g \cos^2 \theta - \gamma + v \tan \theta &= \mu, \\ -g \sin^2 \theta + \gamma + v \cot \theta &= \mu, \end{aligned} \quad (\text{B.14})$$

which can be transformed into the polynomial

$$gy^4 + 4(\gamma + iv)y^3 + 4(-\gamma + iv)y - g = 0 \quad (\text{B.15})$$

by eliminating μ and substituting $y = e^{2i\theta}$. The four solutions of the polynomial can be obtained by any of the methods to solve polynomials of degree four. Once they are known μ can be calculated.

Appendix C. Derivation of the coefficients in the matrix model from the extended Gaussian model

The matrix model (8) can be derived as a discrete nonlinear ansatz of the extended model (for the derivation of a nonlinear discrete Schrödinger equation from the GPE see [46, 57, 58]). We rearrange the terms in (20) which results in

$$i\dot{\psi}_A = \left(\underbrace{-g|\psi_A|^2}_{H_{A0}} \underbrace{-\partial_x^2 + \frac{1}{4}x^2 + V_0^G e^{-\sigma x^2}}_{H_1} \right) \psi_A + \underbrace{i\gamma x e^{-\rho x^2}}_{H_{AB}} \psi_B, \quad (\text{C.1})$$

$$i\dot{\psi}_B = \left(\underbrace{-g|\psi_B|^2}_{H_{B0}} \underbrace{-\partial_x^2 + \frac{1}{4}x^2 + V_0^G e^{-\sigma x^2}}_{H_1} \right) \psi_B + \underbrace{-i\gamma x e^{-\rho x^2}}_{H_{BA}} \psi_A. \quad (\text{C.2})$$

Also a slightly different parametrisation for the ansatz of coupled Gaussians (18) is used

$$\psi_i = \sum_{j=1,2} g_{i,j} = \sum_{j=1,2} d_{i,j}(t) f_{i,j}(x) = \sum_{j=1,2} d_{i,j}(t) e^{a_{i,j}(x-q_{i,j})^2 + p_{i,j}(x-q_{i,j})} \quad (\text{C.3})$$

with $i = A, B$, $j = 1, 2$, $a_{i,j} \in \mathbb{C}$ and $p_{i,j}, q_{i,j} \in \mathbb{R}$. In this new ansatz the amplitude and phase $d_{i,j}$ is separated from the shape $f_{i,j}$ of the wave functions. It is assumed that the shape is constant in time and only the amplitude and phase changes.

In the following paragraphs we only consider the equation of subsystem A the calculation for subsystem B can be done in the same way. We insert the new ansatz (C.3) into (C.2) and obtain

$$\sum_{k=1,2} i\dot{d}_{A,k} = \sum_{k=1,2} (H_A + H_1) d_{A,k} f_{A,k} + H_{AB} d_{B,k} f_{B,k}. \quad (\text{C.4})$$

The equation is multiplied with $f_{A,1}^*$ and $f_{A,2}^*$ from the left and the equation is integrated over x . The resulting two equations can be written as a matrix equation

$$\begin{aligned} i \underbrace{\begin{pmatrix} \langle f_{A,1} | f_{A,1} \rangle & \langle f_{A,1} | f_{A,2} \rangle \\ \langle f_{A,2} | f_{A,1} \rangle & \langle f_{A,2} | f_{A,2} \rangle \end{pmatrix}}_{=K_A} \underbrace{\begin{pmatrix} \dot{d}_{A,1} \\ \dot{d}_{A,2} \end{pmatrix}}_{=\dot{d}_A} \\ = \underbrace{\begin{pmatrix} \langle f_{A,1} | H_A + H_1 | f_{A,1} \rangle & \langle f_{A,1} | H_A + H_1 | f_{A,2} \rangle \\ \langle f_{A,2} | H_A + H_1 | f_{A,1} \rangle & \langle f_{A,2} | H_A + H_1 | f_{A,2} \rangle \end{pmatrix}}_{=G_A} \begin{pmatrix} d_{A,1} \\ d_{A,2} \end{pmatrix} \\ + \underbrace{\begin{pmatrix} \langle f_{A,1} | H_{AB} | f_{B,1} \rangle & \langle f_{A,1} | H_{AB} | f_{B,2} \rangle \\ \langle f_{A,2} | H_{AB} | f_{B,1} \rangle & \langle f_{A,2} | H_{AB} | f_{B,2} \rangle \end{pmatrix}}_{=G_{AB}} \begin{pmatrix} d_{B,1} \\ d_{B,2} \end{pmatrix}. \end{aligned} \quad (\text{C.5})$$

Combining the equations from both subsystems results in a four-dimensional matrix equation

$$i \begin{pmatrix} K_A & 0 \\ 0 & K_B \end{pmatrix} \begin{pmatrix} \dot{d}_A \\ \dot{d}_B \end{pmatrix} = \begin{pmatrix} G_A & G_{AB} \\ G_{BA} & G_B \end{pmatrix} \begin{pmatrix} d_A \\ d_B \end{pmatrix}. \quad (\text{C.6})$$

Table C1. Numerical absolute values of the matrix entries for matrices G_A and G_B for $g = 0.2$ and $\gamma = 0.03$. See figure 6.

	contact interaction H_{A0} and H_{B0}	external potential and kinetic energy H_1
diagonal	7.1214×10^{-2}	4.6221
off-diagonal	2.3891×10^{-4}	8.2474×10^{-2}

We add a numerical example, which is obtained for $g = 0.2$ and $\gamma = 0.03$ for the extended model (compare figure 6).

First we examine the matrices K_A and K_B .

$$K_A = K_B = \begin{pmatrix} 1.87 & 0.027 - 0.0097i \\ 0.027 + 0.0097i & 1.87 \end{pmatrix}. \quad (\text{C.7})$$

It is obvious that the matrix has only small off-diagonal elements since the overlap of the wave functions of different wells is very small. Therefore the matrix K can be approximated by a diagonal matrix D . Then the equation is multiplied with D^{-1} from the left.

Now we examine the matrix elements of the matrix G_{AB} . The first diagonal element of the matrix is

$$-i\gamma \langle f_{A1}^* | x e^{-\rho x^2} | f_{B1} \rangle, \quad (\text{C.8})$$

where the second term in brackets contains only structural information and can be integrated. It corresponds to the fit parameter γ_0 . We examine the numerical values of the matrix

$$G_{AB} = \begin{pmatrix} 9.59 \times 10^{-4} + 6.31 \times 10^{-2}i & 9.40 \times 10^{-5} \\ 9.40 \times 10^{-5} & 9.59 \times 10^{-4} + 6.31 \times 10^{-2}i \end{pmatrix}. \quad (\text{C.9})$$

It is obvious that the small overlap of the wave functions in different wells leads to very small off-diagonal elements, which can be neglected.

The entries of the matrices G_A and G_B consist of terms containing the external potential and the kinetic energy on the one hand and terms containing the contact interaction on the other hand. The terms of the external potential and the kinetic energy in the diagonal element induce a shift of the energy (which corresponds to the offset $\Delta\mu$ in the fit), therefore only the nonlinear contact interaction term remains on the diagonal. The contact interaction in the off-diagonal is very small (compare table C1) when compared to the diagonal, and can be neglected. Therefore in the off-diagonal only the terms from the external potential and the kinetic energy remain. These correspond to the coupling parameter v in the fit.

References

- [1] N. Moiseyev. *Non-Hermitian Quantum Mechanics*. Cambridge University Press, Cambridge, 2011.

- [2] C. M. Bender and S. Boettcher. Real spectra in non-Hermitian Hamiltonians having \mathcal{PT} symmetry. *Phys. Rev. Lett.*, 80:5243–5246, 1998.
- [3] H. F. Jones and Jr. E. S. Moreira. Quantum and classical statistical mechanics of a class of non-Hermitian Hamiltonians. *J. Phys. A*, 43:055307, 2010.
- [4] V. Jakubský and M. Znojil. An explicitly solvable model of the spontaneous \mathcal{PT} -symmetry breaking. *Czech. J. Phys.*, 55:1113, 2005.
- [5] H. Mehri-Dehnavi, A. Mostafazadeh, and A. Batal. Application of pseudo-Hermitian quantum mechanics to a complex scattering potential with point interactions. *J. Phys. A*, 43:145301, 2010.
- [6] C. M. Bender, S. Boettcher, and P. N. Meisinger. \mathcal{PT} -symmetric quantum mechanics. *J. Math. Phys.*, 40:2201, 1999.
- [7] C. E. Ruter, K. G. Makris, R. El-Ganainy, D. N. Christodoulides, M. Segev, and D. Kip. Observation of parity-time symmetry in optics. *Nat Phys*, 6:192–195, 2010. 10.1038/nphys1515.
- [8] I. V. Barashenkov, G. S. Jackson, and S. Flach. Blow-up regimes in the \mathcal{PT} -symmetric coupler and the actively coupled dimer. *Phys. Rev. A*, 88:053817, 2013.
- [9] S. Deffner and A. Saxena. Jarzynski equality in \mathcal{PT} -symmetric quantum mechanics. *Phys. Rev. Lett.*, 114:150601, 2015.
- [10] S. Albeverio, S. Fassari, and F. Rinaldi. The discrete spectrum of the spinless one-dimensional Salpeter Hamiltonian perturbed by δ -interactions. *J. Phys. A*, 48:185301, 2015.
- [11] A. Mostafazadeh. Nonlinear spectral singularities for confined nonlinearities. *Phys. Rev. Lett.*, 110:260402, 2013.
- [12] S. Bittner, B. Dietz, U. Günther, H. L. Harney, M. Miski-Oglu, A. Richter, and F. Schäfer. \mathcal{PT} Symmetry and Spontaneous Symmetry Breaking in a Microwave Billiard. *Phys. Rev. Lett.*, 108:024101, 2012.
- [13] J. Schindler, A. Li, M. C. Zheng, F. M. Ellis, and T. Kottos. Experimental study of active *LRC* circuits with \mathcal{PT} symmetries. *Phys. Rev. A*, 84:040101, 2011.
- [14] J. Schindler, Z. Lin, J. M. Lee, H. Ramezani, F. M. Ellis, and T. Kottos. \mathcal{PT} -symmetric electronics. *J. Phys. A*, 45:444029, 2012.
- [15] A. Ruschhaupt, F. Delgado, and J. G. Muga. Physical realization of \mathcal{PT} -symmetric potential scattering in a planar slab waveguide. *J. Phys. A*, 38:L171, 2005.
- [16] A. Guo, G.J. Salamo, D. Duchesne, R. Morandotti, M. Volatier-Ravat, V. Aimez, G.A. Siviloglou, and D. N. Christodoulides. Observation of \mathcal{PT} -symmetry breaking in complex optical potentials. *Phys. Rev. Lett.*, 103:093902, 2009.
- [17] H. Ramezani, T. Kottos, R. El-Ganainy, and D. N. Christodoulides. Unidirectional nonlinear \mathcal{PT} -symmetric optical structures. *Phys. Rev. A*, 82:043803, 2010.
- [18] Z.H. Musslimani, Konstantinos G. Makris, R. El-Ganainy, and D. N. Christodoulides. Optical solitons in \mathcal{PT} periodic potentials. *Phys. Rev. Lett.*, 100:30402, 2008.
- [19] K. G. Makris, R. El-Ganainy, D. N. Christodoulides, and Z. H. Musslimani. \mathcal{PT} -Symmetric Periodic Optical Potentials. *Int. J. Theo. Phys.*, 50:1019, 2011.
- [20] K. G. Makris, R. El-Ganainy, D. N. Christodoulides, and Z. H. Musslimani. Beam Dynamics in \mathcal{PT} Symmetric Optical Lattices. *Phys. Rev. Lett.*, 100:103904, 2008.
- [21] K. G. Makris, R. El-Ganainy, D. N. Christodoulides, and Z.H. Musslimani. \mathcal{PT} -symmetric optical lattices. *Phys. Rev. A*, 81:063807, 2010.
- [22] K. G. Makris, R. El-Ganainy, D. N. Christodoulides, and Z.H. Musslimani. Beam dynamics in \mathcal{PT} symmetric optical lattices. *Phys. Rev. Lett.*, 100:103904, 2008.
- [23] Y. D. Chong, L. Ge, and A. D. Stone. \mathcal{PT} -symmetry breaking and laser-absorber modes in optical scattering systems. *Phys. Rev. Lett.*, 106:093902, 2011.
- [24] Peng, B and Kaya, Ş. Ö. and Lei, F. and Minufu, F. and Gianfreda, M. and Long, G. L. and Fan, S. and Nori, F. and Bender, C. M. and Yang, L. Parity-time-symmetric whispering-gallery microcavities. *Nat Phys*, 10:394–398, 2014. 10.1038/nphys2927.
- [25] D. Dast, D. Haag, H. Cartarius, and G. Wunner. Quantum master equation with balanced gain

- and loss. *Phys. Rev. A*, 90:052120, 2014.
- [26] S. Klaiman, U. Günther, and N. Moiseyev. Visualization of Branch Points in \mathcal{PT} -Symmetric Waveguides. *Phys. Rev. Lett.*, 101:080402, 2008.
- [27] E.-M. Graefe. Stationary states of a \mathcal{PT} symmetric two-mode Bose–Einstein condensate. *J. Phys. A*, 45:444015, 2012.
- [28] E. M. Graefe, U. Günther, H. J. Korsch, and A. E. Niederle. A non-Hermitian \mathcal{PT} symmetric Bose-Hubbard model: eigenvalue rings from unfolding higher-order exceptional points. *J. Phys. A*, 41:255206, 2008.
- [29] W. D. Heiss, H. Cartarius, G. Wunner, and J. Main. Spectral singularities in \mathcal{PT} -symmetric Bose–Einstein condensates. *J. Phys. A*, 46:275307, 2013.
- [30] L. P. Pitaevskii and S. Stringari. *Bose-Einstein Condensation*. Oxford University Press, 2003.
- [31] A. Mostafazadeh. Delta-function potential with a complex coupling. *J. Phys. A*, 39:13495, 2006.
- [32] H. F. Jones. Interface between Hermitian and non-Hermitian Hamiltonians in a model calculation. *Phys. Rev. D*, 78:065032, 2008.
- [33] A. Mostafazadeh and H. Mehri-Dehnavi. Spectral singularities, biorthonormal systems and a two-parameter family of complex point interactions. *J. Phys. A*, 42:125303, 2009.
- [34] T. Mayteevarunyoo, B. A. Malomed, and G. Dong. Spontaneous symmetry breaking in a nonlinear double-well structure. *Phys. Rev. A*, 78:053601, 2008.
- [35] K. Rapedius and H. J. Korsch. Resonance solutions of the nonlinear Schrödinger equation in an open double-well potential. *J. Phys. B*, 42:044005, 2009.
- [36] D. Witthaut, K. Rapedius, and H. J. Korsch. The nonlinear Schrödinger equation for the delta-comb potential: quasi-classical chaos and bifurcations of periodic stationary solutions. *JNMP*, 16:207, 2008.
- [37] S. Fassari and F. Rinaldi. On the Spectrum of the Schrödinger Hamiltonian of the One-Dimensional Harmonic Oscillator Perturbed by Two Identical Attractive Point Interactions. *Rep. Math. Phys.*, 69:353, 2012.
- [38] E. Demiralp. Bound states of n -dimensional harmonic oscillator decorated with Dirac delta functions. *J. Phys. A*, 38:4783, 2005.
- [39] H.F. Jones. The energy spectrum of complex periodic potentials of the Kronig-Penney type. *Phys. Lett. A*, 262:242, 1999.
- [40] Z. Ahmed. Energy band structure due to a complex, periodic, \mathcal{PT} -invariant potential. *Phys. Lett. A*, 286:231, 2001.
- [41] H. Uncu, D. Tarhan, E. Demiralp, and Ö. E. Müstecaplıoglu. Bose-Einstein condensate in a harmonic trap with an eccentric dimple potential. *Las. Phys.*, 18:331, 2008.
- [42] H. Cartarius and G. Wunner. Model of a \mathcal{PT} -symmetric Bose-Einstein condensate in a δ -function double-well potential. *Phys. Rev. A*, 86:013612, 2012.
- [43] D. Dast, D. Haag, H. Cartarius, Günter Wunner, R. Eichler, and J. Main. A Bose-Einstein condensate in a \mathcal{PT} -symmetric double well. *Fortschritte der Physik*, 61:124–139, 2013.
- [44] D. Haag, D. Dast, A. Löhle, H. Cartarius, J. Main, and G. Wunner. Nonlinear quantum dynamics in a \mathcal{PT} -symmetric double well. *Phys. Rev. A*, 89:023601, 2014.
- [45] M. Kreibich, J. Main, H. Cartarius, and G. Wunner. Hermitian four-well potential as a realization of a \mathcal{PT} -symmetric system. *Phys. Rev. A*, 87:051601(R), 2013.
- [46] M. Kreibich, J. Main, H. Cartarius, and G. Wunner. Realizing \mathcal{PT} -symmetric non-Hermiticity with ultracold atoms and Hermitian multiwell potentials. *Phys. Rev. A*, 90:033630, 2014.
- [47] F. Single, H. Cartarius, G. Wunner, and J. Main. Coupling approach for the realization of a \mathcal{PT} -symmetric potential for a Bose-Einstein condensate in a double well. *Phys. Rev. A*, 90:042123, 2014.
- [48] K. Li, P. G. Kevrekidis, B. A. Malomed, and U. Günther. Nonlinear \mathcal{PT} -symmetric plaquettes. *J. Phys. A*, 45:444021, 2012.
- [49] J. Yang. Partially \mathcal{PT} symmetric optical potentials with all-real spectra and soliton families in multidimensions. *Opt. Lett.*, 39:1133–1136, 2014.

- [50] S. V. Suchkov, S. V. Dmitriev, B. A. Malomed, and Y. S. Kivshar. Wave scattering on a domain wall in a chain of \mathcal{PT} -symmetric couplers. *Phys. Rev. A*, 85:033825, 2012.
- [51] F. Kh. Abdullaev, Y. V. Kartashov, V. V. Konotop, and D. A. Zezyulin. Solitons in \mathcal{PT} -symmetric nonlinear lattices. *Phys. Rev. A*, 83:41805, 2011.
- [52] S. Rau, J. Main, and G. Wunner. Variational methods with coupled Gaussian functions for Bose-Einstein condensates with long-range interactions. I. General concept. *Phys. Rev. A*, 82:023610, 2010.
- [53] S. Rau, J. Main, H. Cartarius, P. Köberle, and G. Wunner. Variational methods with coupled Gaussian functions for Bose-Einstein condensates with long-range interactions. II. Applications. *Phys. Rev. A*, 82:023611, 2010.
- [54] A. D. McLachlan. A variational solution of the time-dependent Schrodinger equation. *Mol. Phys.*, 8:39–44, 1964.
- [55] G. Theocharis, P. G. Kevrekidis, D. J. Frantzeskakis, and P. Schmelcher. Symmetry breaking in symmetric and asymmetric double-well potentials. *Phys. Rev. E*, 74:056608, 2006.
- [56] Y. A. Kuznetsov. *Elements of Applied Bifurcation Theory*, volume 112 of *Applied Mathematical Sciences*. Springer-Verlag, third edition, 2004.
- [57] A. Trombettoni and A. Smerzi. Discrete Solitons and Breathers with Dilute Bose-Einstein Condensates. *Phys. Rev. Lett.*, 86:2353–2356, 2001.
- [58] A. Smerzi and A. Trombettoni. Nonlinear tight-binding approximation for Bose-Einstein condensates in a lattice. *Phys. Rev. A*, 68:023613, 2003.